Compressive deformation of rolled AZ80 magnesium alloy along different material orientations

Ying Xiong & Yanyao Jiang

Journal of Materials Science

ISSN 0022-2461 Volume 55 Number 9

J Mater Sci (2020) 55:4043-4053 DOI 10.1007/s10853-019-04238-5



Your article is protected by copyright and all rights are held exclusively by Springer Science+Business Media, LLC, part of Springer Nature. This e-offprint is for personal use only and shall not be self-archived in electronic repositories. If you wish to selfarchive your article, please use the accepted manuscript version for posting on your own website. You may further deposit the accepted manuscript version in any repository, provided it is only made publicly available 12 months after official publication or later and provided acknowledgement is given to the original source of publication and a link is inserted to the published article on Springer's website. The link must be accompanied by the following text: "The final publication is available at link.springer.com".



Metals & corrosion



Compressive deformation of rolled AZ80 magnesium alloy along different material orientations

Ying Xiong^{1,*} o and Yanyao Jiang²

Received: 11 October 2019 Accepted: 19 November 2019 Published online: 25 November 2019

© Springer Science+Business Media, LLC, part of Springer Nature 2019

ABSTRACT

The compressive deformation behavior of a rolled AZ80 magnesium alloy was experimentally studied with testing specimens taken from a thick plate at five different material orientations with respect to the normal direction (ND): 0° (ND), 30° , 45° , 60° , and 90° (RD). The experimental results reveal a strong anisotropy in the mechanical properties of the textured material. The macrotexture of specimens interrupted at different strains was examined by X-ray diffractometer. The correlation between the initial texture, the mechanical anisotropy, and the activation of different deformation modes was analyzed. The initial crystal orientation has a decisive effect on the operation of twinning and slip modes. The strength of initial texture also plays an important role in the evolution of microstructure.

Introduction

The emission of carbon dioxide in the vehicle has seriously damaged the human living environment. Reduction in the weight of the vehicles will effectively improve fuel efficiency, thus reducing the greenhouse gas emissions. Magnesium alloys, as the lightest structural metal, have a low weight, high strength/weight ratio, and excellent machinability. These advantages make them attractive structural materials.

Wrought magnesium alloys have better mechanical properties than the cast magnesium alloys. A wrought magnesium alloy usually forms a strong (0001) $\langle 10\bar{1}1 \rangle$ basal texture after the extrusion or rolling process. When a magnesium alloy is loaded in

different directions, the material shows obvious anisotropy of mechanical properties. The stress-strain curves are asymmetrical under uniaxial tension and compression [1–4]. The significant anisotropy is attributed to different deformation modes occurring during tensile and compressive deformation. The deformation mechanisms of the magnesium alloy with hexagonal close-packed crystal structure are basal slip, prismatic slip, pyramidal slip, and tension/contraction twinning [5, 6]. During deformation at room temperature, the critical resolved shear stress (CRSS) for prismatic and pyramidal slips is much higher than that for basal slip and tension twinning. Tension twinning is activated when there is tension loading parallel to the *c*-axes or compression loading perpendicular to the *c*-axes [7–9]. Therefore, the

Address correspondence to E-mail: yxiong@zjut.edu.cn



¹College of Mechanical Engineering, Zhejiang University of Technology, Hangzhou 310032, Zhejiang, China

²Department of Mechanical Engineering, University of Nevada, Reno, Reno, NV 89557, USA

mechanical anisotropy of wrought magnesium alloys is closely related to the loading direction with respect to the original texture.

Structural components made from magnesium alloys can be subjected to loading in different directions. Therefore, it is important to understand the anisotropic deformation behavior of the material. Many researchers have investigated the effect of loading direction with respect to the material orientation on the deformation behavior of rolled magnesium alloy sheet [1, 10-12]. However, these studies are limited to two typical directions of rolled plate: rolling direction (RD) and tangential direction (TD). In the present study, the compression deformation behavior of rolled AZ80 magnesium alloy thick plate along five loading directions is studied. Testing specimens are taken from the plate at 0° , 30° , 45° , 60° , and 90° with respect to the normal direction (ND). X-ray diffractometer (XRD) is employed to examine the development of macrotexture at different strain levels during compressive loading. The effect of material orientations on the deformation behavior is discussed.

Experimental method

Material and specimen

The material used in the study is a hot-rolled AZ80 magnesium alloy plate with a thickness of 60 mm. The original microstructure of the material was reported in an earlier publication [13]. The material has an equiaxial grain structure with an average grain size of approximate 50 μm and β-Mg₁₇Al₁₂ phases distributing along the grains boundary (αmatrix). The initial texture of the material measured by X-ray diffraction (XRD) on the RD-TD plane is shown in Fig. 1. $\{0002\}, \{10\overline{1}0\}$ and $\{10\overline{1}1\}$ pole figures indicate that the c-axes of most grains are parallel to the ND and the a-axes are randomly distributed on the RD-TD rolled plane. The {0002} pole figure shows that the area of the texture cluster gathered in the center is larger, suggesting that the *c*axes of most grains are not completely perpendicular to the rolled plane.

Dog-bone-shaped specimens were cut from the thick plate for monotonic compression experiments. The specimen has a diameter of 10 mm within a gauge length of 15 mm. The angles between the axial

direction of the specimens and the normal direction (ND) are 0° (ND), 30° (ND30), 60° (ND60), 90° (RD and TD) as shown in Fig. 2. Schematics of HCP unit cells are presented in Fig. 2. Before testing, the outer surface in the gauge section of the specimen was polished by using silicon carbide papers with grit no. from 400 up to 1200.

Experiments

All the experiments were carried out using a computer-controlled servo-hydraulic material testing system in ambient air. The strain rate was controlled at approximate 6.0×10^{-3} /s. A specimen was loaded to a predefined strain level for the study of the microstructure evolution during compressive deformation. For the ND specimens, experiments were interrupted at strains of 2%, 5%, 7%, and 9.8% (fracture), respectively. For the ND30 specimens, experiments were terminated at strains of 3%, 9%, and 13.7% (fracture), respectively. The ND45 specimens were loaded to 2%, 8%, and 18.7% (fracture). The ND60, RD, and TD specimens were carried out until failure. The macrotexture of the specimens interrupted at different strains was examined by XRD. All the samples were measured on the RD-TD planes. $\{0002\}, \{10\overline{10}\}\$ and $\{10\overline{11}\}\$ pole figures were calculated using the Tex Tools software.

Results and discussion

Macroscopic mechanical behavior

The stress-strain curves under monotonic compression for different orientation specimens are shown in Fig. 3, and the mechanical properties are summarized in Table 1. The stress–strain curves are strongly dependent on the material orientation. Similar results were obtained by testing a semi-closed die-forged AZ80 extrusion [14]. The stress–strain curves in the specimens (ND, ND30, and ND45) less than 45° show concave-down shapes (Fig. 3a), whereas the stressstrain curves of the specimens gradually show sigmoidal shapes (Fig. 3b) with the direction angle increasing from 60° (ND60) to 90° (RD and TD). The elongations are dependent on the material orientation. The RD specimen (20.6%) exhibits a highest elongation among all the orientation specimens, whereas the ND specimen has the lowest elongation



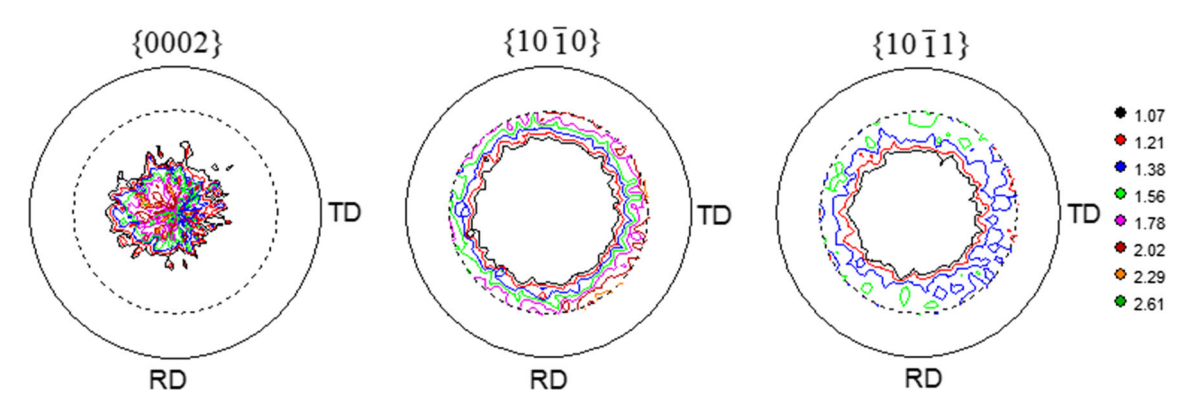


Figure 1 (0002), $\{10\overline{1}0\}$ and $\{10\overline{1}1\}$ pole figures of the initial material measured by XRD.

Figure 2 Schematics of specimen geometries and approximate texture.

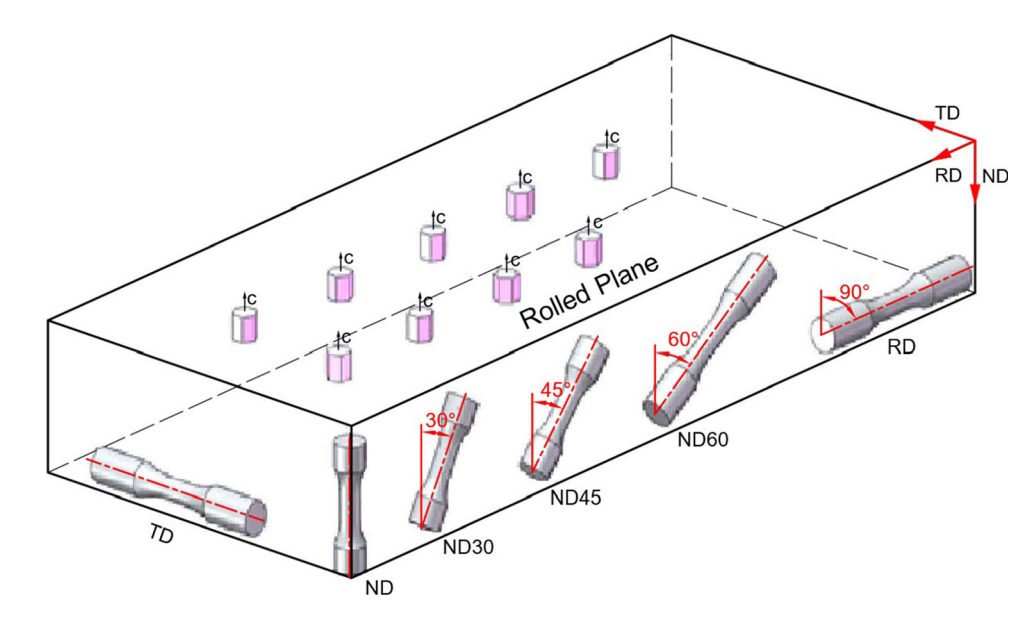
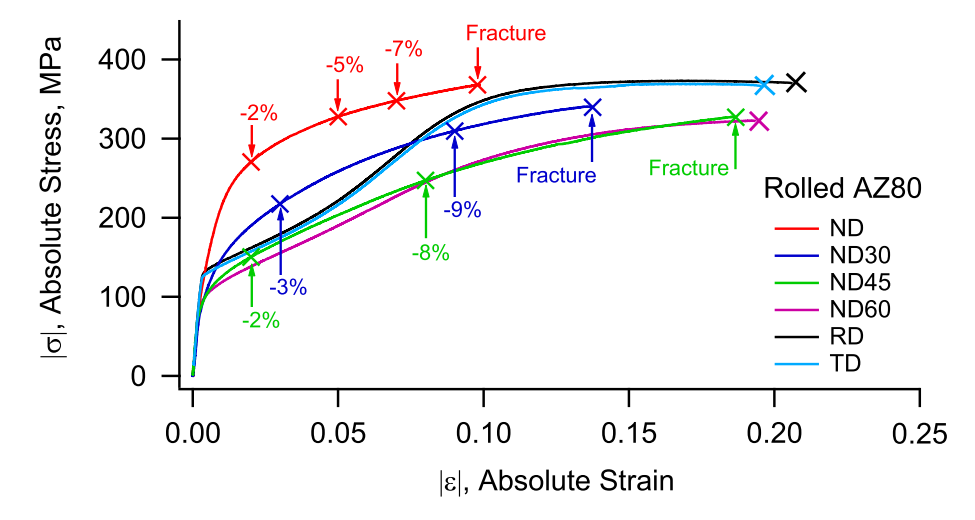


Figure 3 Stress–strain curves of rolled AZ80 Mg alloy under monotonic compression in different material orientations.



(9.8%). The 0.2% offset yield stress and the true fracture strength of the material do not increase with increasing direction angle. Both the compressive

yield stress and the fracture stress in the ND (155 MPa/367 MPa), ND30 (100 MPa/340 MPa) and ND45 (98 MPa/327 MPa) specimens gradually



Table 1 Mechanical properties of different material orientations under monotonic compression

Mechanical properties in compression	ND	ND30	ND45	ND60	RD	TD
0.2% offset yield stress, σ_{yc} (MPa)	154.9 367.0	100.3 339.6	98.4 327.0	98.0 322.0	133.7 369.8	129.4 366.0
True fracture stress, σ_{fc} (MPa) Elongation (%)	9.8	13.7	18.7	19.4	20.6	19.6

decrease with the direction angle increasing from 0° to 45° , whereas those in the ND60 (98 MPa/322 MPa) and RD (134 MPa/370 MPa) specimens increase with the direction angle increasing from 60° to 90° . The elongation (19.6%), yield strength (129 MPa), and fracture strength (366 MPa) in the TD specimen are slightly lower than those in the RD. The results may be associated with the non-uniform distribution of the Mg₁₇Al₁₂ phase [15]. Similar compressive yield strength occurs in the ND30, ND45 and ND60 specimens.

Figure 4 shows the variations of strain hardening rate with the strain in different material orientations. For the specimens with a direction angle less than 45°, the hardening rate curve can be divided into two stages as shown in Fig. 4a. In Stage I, the strain hardening rate rapidly decreases with increasing strain. As the direction angle increasing from 0° (ND) to 45° (ND45), the decreasing slope of strain hardening rate increases. In Stage II, the strain hardening rate slowly decreases with increasing strain, and the stain value at fracture point increases with increasing direction angle. For the specimens with a direction angle large than 60°, the hardening rate curves can be divided into three stages as shown in Fig. 4b. In Stage I, the hardening rate rapidly decreases with increasing strain, and the decreasing slope increases with direction angle increasing from 60° (ND60) to 90° (RD). In Stage II, the hardening rate curve in the ND60 specimen reveals a peculiar characteristic, where the strain hardening rate remains almost constant. However, the hardening rate gradually increases with increasing strain as the direction angle reaches 90° (RD). In Stage III, the hardening rate continually decreases with increasing strain. The decreasing degree of hardening rate in the RD specimen is higher than that in the ND60 specimen. The results suggest that deformation mechanisms are involved at different strain levels for a given material orientation. The different deformation behavior with strain is related to the texture evolution during compressive deformation, which will be discussed.



Texture evolution

The stress–strain curve in the RD is similar to those of other rolled AZ systems of magnesium alloys, and the deformation mechanisms have been reported by many researchers [1, 2, 4, 9, 12]. The compressive deformation behavior of ND45 specimen is similar to that of ND60 specimen. Consequently, ND, ND30 and ND45 specimens are selected to be analyzed for the macrotexture evolution during compressive loading.

Figure 5 shows the macrotextures $\{0002\}, \{10\bar{1}0\}$, and $\{10\bar{1}1\}$ diffraction peaks in the ND specimens at different strain levels. For the ND specimen, the activation of $\{10\overline{1}2\}$ tension twinning is difficult because the compressive loading is parallel to the *c*-axes of the grains. With the compressive strain increasing from 2 to 7%, the change of macroscopic texture during compressive deformation is very small (Fig. 5a). In addition, $\{0002\}, \{10\overline{10}\}$, and {1011} diffraction peaks are almost unchanged (Fig. 5b). The texture density increases from 2.06 to 3.29 when the compressive strain increases from 0 to 7%, and the texture cluster is gathered in the center of the (0002) pole figure. Although the $\{10\overline{1}1\}$ contraction twinning or $\{10\overline{1}1\} - \{10\overline{1}2\}$ double twinning may be formed at the later stage of compression, the effect of twins on texture is insignificant due to low volume fraction occupied by these possible contraction twins [6, 16, 17]. The increase in texture density is due to basal slips because of the misorientations of the grains in the rolled plate and the activation of the non-basal slips [6].

Figure 6 shows the macrotexture and $\{0002\}, \{10\bar{1}0\}$ and $\{10\bar{1}1\}$ diffraction peaks in the ND30 specimens at different strain levels. At a compressive strain of 3%, the texture cluster moves from the center to the RD direction in the (0002) pole figure, and the texture intensity increases from an original value of 2.06 to 5.76 (Fig. 6a). The (0002) peak decreases rapidly, and $(10\bar{1}1)$ peak increases (Fig. 6b). The macroscopic mechanical properties

Figure 4 Strain hardening rate curves of rolled AZ80 Mg alloy of different material orientations under compression.

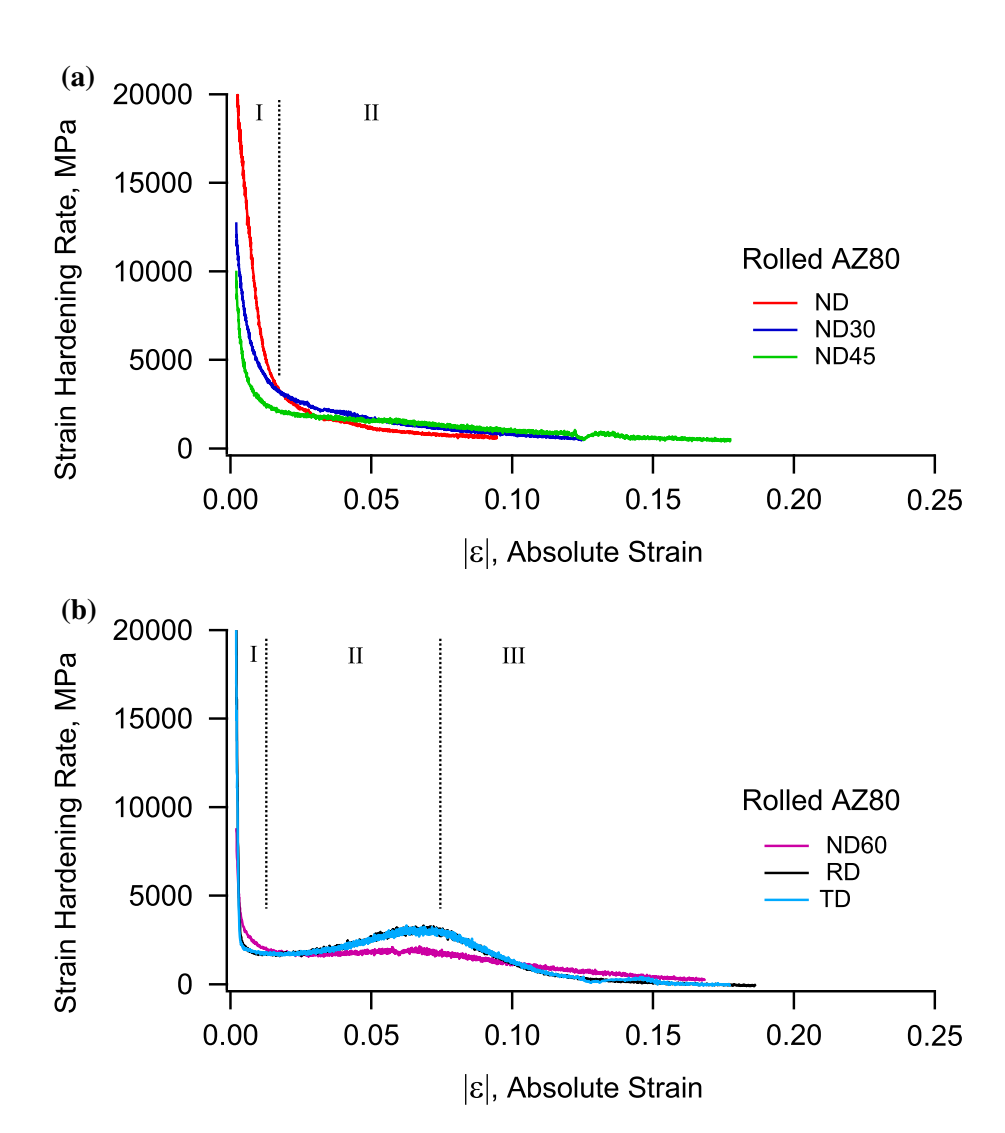


(Fig. 1 and Table 1) indicate that the yield strength in the ND30 specimen is much lower than those in the RD and TD specimens. The texture evolution in Fig. 6a suggests that no twinning occurs at a lower strain. The critical resolved shear stress (CRSS) of basal slip is lower than the activation stress for tension twinning at room temperature [18]. It is inferred that the early deformation mechanism in the ND30 specimens is dominated by basal <a> slips. The result is consistent with the observation made earlier [19]. With the compressive strain increases from 3 to 9%, the texture density increases from 5.76 to 7.01 (Fig. 6a). In addition, the (0002) peak increases and the $(10\bar{1}1)$ peak is virtually unchanged (Fig. 6b). The results indicate that the prismatic <a> slips occur at this deformation stage [6]. When the compressive strain increases from 9% to fracture, the second texture cluster appears in the (0002) pole figure, while

the first texture cluster moves toward the center (Fig. 6a). The texture intensity decreases from 7.01 to 5.5. The (0002) peak increases and the ($10\bar{1}1$) peak decreases. Such results suggest that the second newly formed texture cluster may be related to the formation of $\{10\bar{1}2\}$ tension twinning. $\{10\bar{1}2\}$ tension twinning has more nucleation sites at higher compressive strains [20]. It indicates that the volume fraction of $\{10\bar{1}2\}$ tension twinning increases with the strain increasing. The twin rotates the grain by 86°, which is favorable for basal <a2 and pyramidal <c4 a> slips. As a result, the first texture group shifts to the center in the (0002) pole figure [4, 10].

Figure 7 shows the macrotexture and $\{0002\}, \{10\bar{1}0\}$ and $\{10\bar{1}1\}$ diffraction peaks in the ND45 specimens at different strain levels. At a compressive strain of 2%, the original texture cluster gathers at the center which deviates to the RD



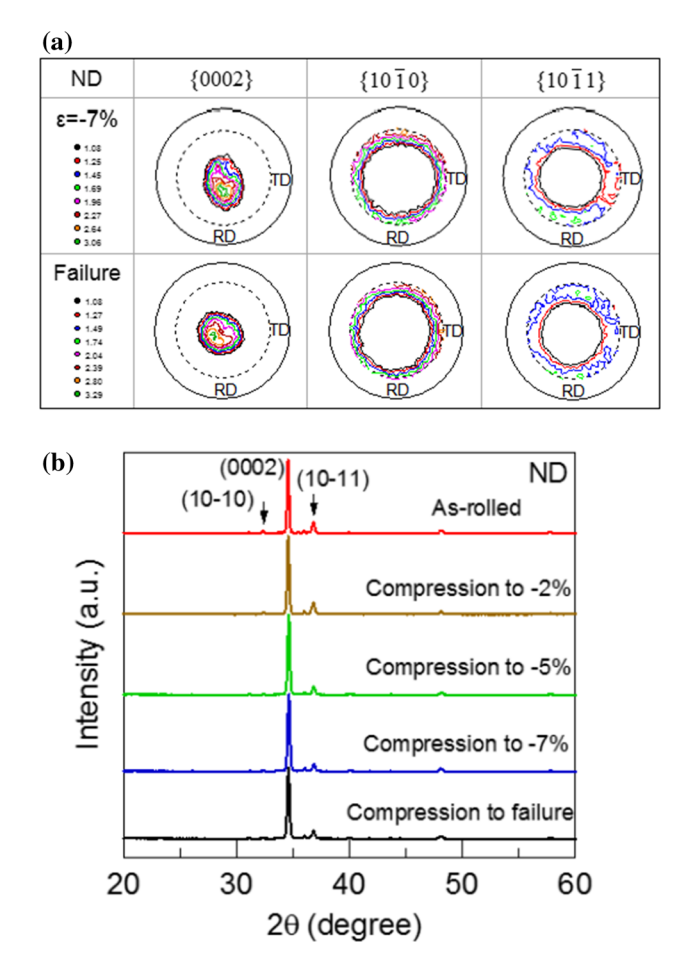


Figure 5 Texture evolution and XRD scans at different strain levels in the ND specimen.

direction, and a weak texture cluster appears in the {0002} pole figure. The texture intensity increases from 2.61 to 5.38. The (0002) diffraction peak in the corresponding 20 diagram is greatly decreased, and the $(10\bar{1}1)$ peak is significantly increased. For the ND45 specimen, the angle between c-axes of most crystals and the loading direction is 45°. In this case, the Schmid factor of basal <a> slip is relatively large [21]. The compressive yield stress of the ND45 specimen is the lowest among the five material orientations, indicating that the basal <a> slip is the easiest deformation mode in the early stage of deformation. When the strain is increased to 8%, the intensity of the first texture cluster decreases and the second texture cluster increases. The comprehensive intensity of texture decreases from 5.38 to 4.90. Accordingly, the (0002) diffraction peak decreases further, and the (1011) peak keeps increasing. As mentioned earlier, the formation of the second texture cluster is related to the activation of $\{10\overline{1}2\}$ tension twinning.

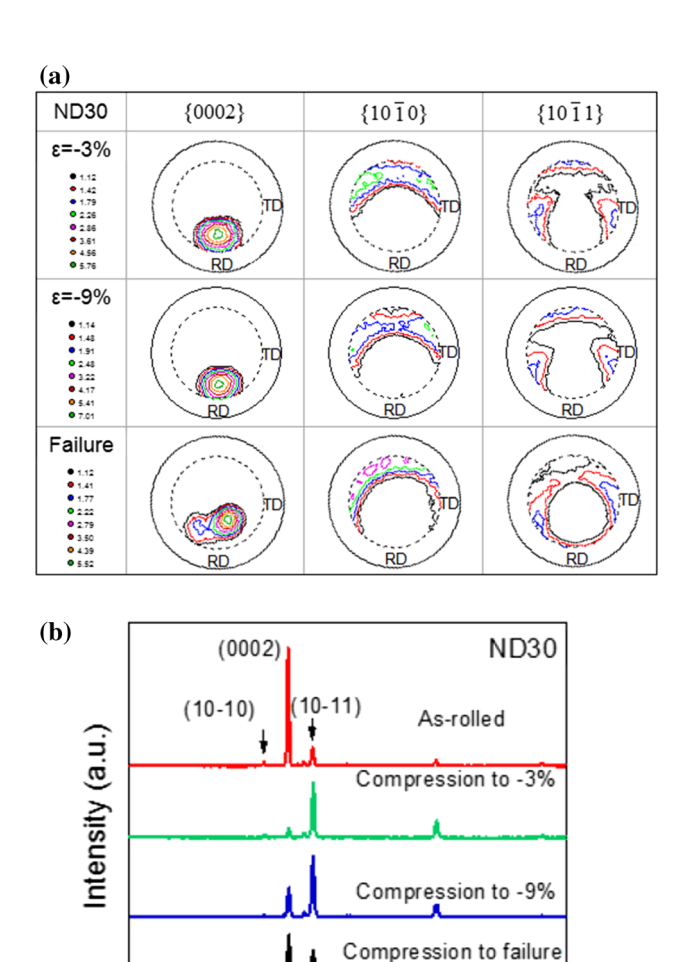


Figure 6 Texture evolution and XRD scans at different strain levels in the ND30 specimen.

40

2θ (degree)

50

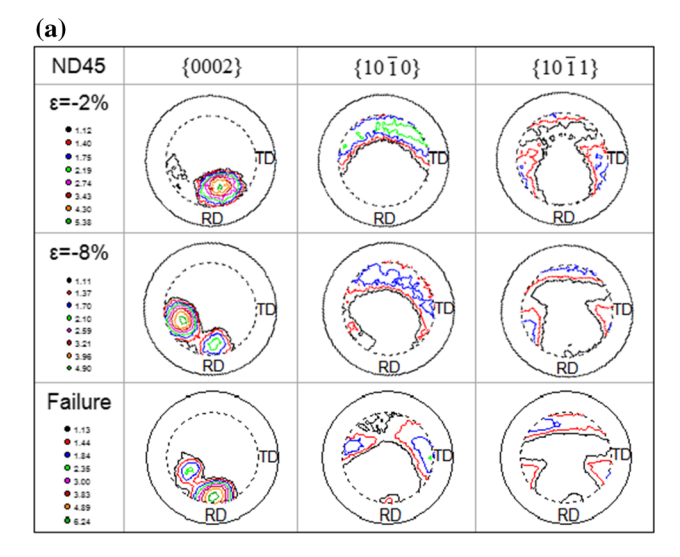
60

20

30

The intensity of the second texture cluster increases and the (0002) diffraction peak decreases, indicating that the $\{10\overline{12}\}$ tension twinning increases with the strain increasing from 2 to 8%. When the ND45 specimen is compressed to fracture, the intensity of the first texture cluster increases and it moves to the center in the (0002) pole figure. In contrast, the intensity of the second texture cluster decreases and it moves to the RD. The texture intensity increases from 4.90 to 6.30. The (0002) diffraction peak increases slightly, while the $(10\bar{1}1)$ peak decreases slightly. Among the large number of twins generated, partially twinned grains move slowly toward the RD (i.e., compression axis) by the basal <a> slips (the second texture cluster), while pyramidal $\langle c + a \rangle$ slips are activated in other twinned grains to





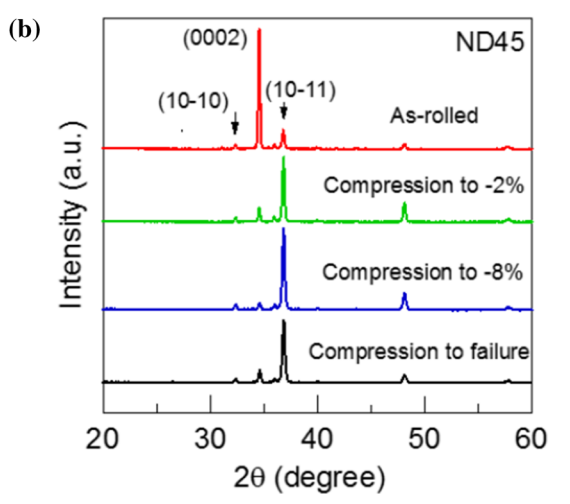


Figure 7 Texture evolution and XRD scans at different strain levels in the ND45 specimen.

accommodate plastic deformation (the first texture cluster).

Comparing the mechanical properties of ND45 with those of the ND60 specimens, similar yield stresses were observed. Therefore, the deformation mechanism leading to yielding should be the same. Previous studies suggest that the $\{10\bar{1}2\}$ tension twinning is more likely to occur in the ND60 samples, while the basal <a> slips present in the ND45 specimen in the early stage of deformation [19, 22, 23]. For the AZ80 Mg alloy under the current investigation, the dispersion angle of the basal plane texture is larger in the direction perpendicular to the compressive stress (Fig. 1). Koike et al. [10] pointed out that the texture intensity can change the dominant deformation mechanism in addition to the crystal

orientation. Therefore, the lower compressive yield stress in the ND60 specimen is a result of the easy activation of basal <a> slips. The stress–strain curve of the ND60 specimen between the yield point and 8% strain is characterized by a concave-up shape (Fig. 3). This characteristic is related to the formation of {1012} tension twinning [1, 2, 4, 5, 7–9, 11, 24]. It is inferred that the volume fraction of {1012} tension twinning increases with the orientation angle increasing from 45° to 60°. When the strain is larger than 8%, the stress-strain curves of the ND45 and ND60 specimens are almost identical. The results suggest exhaustion of $\{10\overline{1}2\}$ tension twinning when the strain reaches 8%. In the ND45 specimen, basal < a > slips and pyramidal < c + a > slips play an important role in the subsequent deformation. This is the reason why the stress-strain curves also look very similar at the later stage of deformation in all the specimens with different material orientations. For the RD specimen, the initial crystal orientation is favorable to $\{10\overline{1}2\}$ tension twinning because the *c*axes of the grains are mostly parallel to the compression direction. Therefore, a large number of $\{10\overline{12}\}\$ tension twins are formed in the initial stage of deformation. In the later stage of deformation, basal < a > slips and pyramidal < c + a > slips play an important role. Therefore, with increasing volume fraction of {1012} tension twinning related to the orientation angle, the strain hardening rate curve shows three distinct characteristic stages in the RD specimen (Fig. 4b). In conclusion, the initial crystal orientation has a decisive effect on the operation of twinning and slip modes during the deformation of magnesium alloy. The initial texture intensity also plays an important role in the activation of certain deformation modes.

Deformation mechanism

Effect of initial crystal orientation on deformation behavior

The stress-strain curves obtained from testing specimens with orientation angle less than 45° show similar characteristics. The strain hardening curves are divided into two stages, and the deformation mechanism in each stage is different (Fig. 4a). The result is consistent with the earlier work [25]. The yield stress is related to the critical shear stress (CRSS) of slip or twinning. The CRSS values of prismatic <a> slip



(10 - 45 MPa), pyramidal < c + a > slip (30 - 80 MPa), and contraction twinning (30 -100 MPa) are higher than those of basal <a> slip (0.45–0.81 MPa) and tension twinning (2 –2.8 MPa). For the ND specimens, prismatic <a> slips with higher CRSS may be activated due to the crystallographic c-axes perpendicular to the compression loading direction [6, 26]. When plastic deformation is dominated by non-basal slips, the material exhibits a higher yield stress (Fig. 3a). Therefore, strain hardening rate decreases rapidly with strain in the early stage of deformation (stage I). As the strain increases continuously, pyramidal $\langle c + a \rangle$ slip is activated to conform to further plastic strain. In the case of $\langle c + a \rangle$ slip, (1011) contraction twinning and $\{10\overline{1}1\} - \{10\overline{1}2\}$ double twinning have an effect on rotating the basal planes toward a more favorable orientation for basal slips [27–30]. Therefore, a low strain hardening rate appears in the later stage of deformation (stage II).

For the ND30 and ND45 specimens, the deformation behavior depends on the competition between slip and twinning. Both twinning and slip are activated during plastic deformation, but the proportion of twinning and slip activated in the different orientation specimens is different. The results of texture analysis show that the dominant deformation mechanism in the ND30 and ND45 specimens is basal <a> slip. When the strain is less than 2%, basal <a> slip dominates deformation in the ND30 specimen. However, some twins are involved in plastic deformation in addition to basal <a> slip in the ND45 specimen. The two deformation mechanisms cause the strain hardening rate to decrease rapidly with the strain in the early stage of deformation. The strain hardening rate in the ND45 specimen decreases more rapidly than that in the ND30 specimen in Stage I (Fig. 4a). With increasing strain, the $\{10\overline{1}2\}$ tension twins are nucleated gradually, and the volume fraction of the twins formed in the ND45 specimen is higher than that in the ND30 specimen. The twined grains are favorable to the activation of slip systems. On the other hand, the twin boundary acts as a barrier to dislocation slips. The interaction of twinning and slip makes the strain more difficult and thus a slowly decreasing strain hardening rate with the strain increasing in Stage II. A higher volume fraction of $\{10\overline{12}\}$ tension twinning results in a greater twinning-slip interaction. Therefore, the strain hardening rate in the ND45 specimen is lower than that of ND30 specimen in the early deformation of Stage II (Fig. 4a). When the twins are saturated, pyramidal $\langle c + a \rangle$ slip becomes the dominant deformation mechanism together with basal $\langle a \rangle$ slip in the twinned grains. This is the reason why the stress–strain curves in the ND30 and ND45 specimens are similar in the later deformation of Stage II.

For specimens with an orientation greater than 60°, the strain hardening curve can be divided into three stages (Fig. 4b). The amount of twins activated increases with the orientation angle. The occurrence of {1012} tension twinning first releases the stress concentration during deformation [31, 32]. Therefore, the strain hardening rate in Stage I shows a rapidly decreasing shape (Fig. 4b). With increasing strain, {1012} tension twinning accumulates and the grains change from a soft orientation to a hard orientation [20]. During plastic deformation, the grain re-orientation caused by $\{10\overline{12}\}$ tension twinning is favorable for prismatic <a> slip [33, 34]. On the one hand, the large number of twin boundaries also act as barriers to dislocation motion, which enhances the strain hardening rate [35]. Therefore, the interaction between twinning and slip results in a significant increase in the strain hardening rate in Stage II. Because the volume fraction of $\{10\overline{1}2\}$ tension twinning in the ND60 specimen is less than that in the RD specimen, it is not enough to cause rapid strain hardening. Therefore, the strain hardening rate in the ND60 specimen is lower than that in the RD specimen in Stage II. When strain reaches approximately 8%, the $\{10\overline{12}\}$ tension twinning consumes the entire grains, and thus, the *c*-axes of these grains are parallel to the loading direction during further compressive loading. In this case, pyramidal $\langle c + a \rangle$ slips are activated. For the RD specimen, {1011} contraction twinning may be formed in the matrix of $\{10\overline{12}\}$ tension twinning to accommodate further deformation [36–38]. The (1011) contraction twinning and $(10\overline{1}1)$ - $\{10\overline{1}2\}$ double twinning have the effect of rotating the basal planes toward a more favorable orientation for basal slips, which likely leads to strain softening [27–29]. The combination of the aforementioned deformation mechanisms leads to a rapid decrease in strain hardening rate in Stage III.



Effect of initial texture intensity on deformation behavior

Theoretically, the ND45 specimen is more favorable for basal <*a*> slips. However, the yield stresses in the ND30, Nd45, and ND60 specimens are similar (Table 1). This indicates that the intensity of texture plays an important role during deformation in addition to the initial crystal orientation. According to the relationship between material orientation and loading direction, ND30 and ND60 specimens have similar capacity in basal <a>> slips. For the AZ80 magnesium alloy under the current investigation, there is a large dispersion angle in the basal plane texture relative to the compression loading direction, resulting in more grains favorable for the basal <a> slip (Fig. 1). Therefore, early deformation of the three specimens is dominated by the basal <a> slip of low CRSS.

Beyond the yield point, the strain hardening rate increases with the increase in orientation angle in Stage II. Because the work hardening behavior in Stage II is related to $\{10\bar{1}2\}$ tension twinning, the twin volume fraction determines the degree of work hardening [31, 36]. Some studies have shown that the slip can induce the formation of variant twins [39]. In the specimens with an orientation angle between 30° and 60°, the factors leading to twin variant nucleation are diverse. In summary, the volume fraction of $\{10\bar{1}2\}$ tension twinning is the main factor affecting the strain hardening rate in Stage II. Since the deformation behavior in Stage II is caused by $\{10\bar{1}2\}$ tension twinning, the length of Stage II is also determined by the twin volume fraction.

Conclusions

The anisotropic compressive deformation behavior of a rolled AZ80 magnesium alloy was experimentally investigated with five different material orientations. Major conclusions are summarized as follows.

- The rolled magnesium alloy exhibits a strong anisotropy in the mechanical properties. The strain hardening curve shows different characteristics. The anisotropic behavior is due to the initial crystal orientation and the choice of deformation mechanisms between slip and twinning.
- 2. When the initial crystal orientation of the specimens (ND, ND30 and ND45) is not favorable for

- the activation of $\{10\overline{1}2\}$ tension twinning, the strain hardening curve shows two features. The strain hardening rate rapidly decreases in Stage I and slowly decreases in Stage II with increasing strain.
- 3. When the initial crystal orientation of specimens (ND60 and RD) is favorable for the activation of $\{10\bar{1}2\}$ tension twinning, the strain hardening curve exhibits three distinct stages. In Stage II, the strain hardening rate increases with increasing strain, and it arises from the texture hardening caused by $\{10\bar{1}2\}$ tension twinning. A decrease in strain hardening rate occurs in Stages I and III.
- 4. The initial crystal orientation affects the competition between twinning and slip, and the deformation behavior depends on the activation of twin and slip. When the orientation angle is less than 45°, slips play an important role. When the orientation angle is greater than 45°, twinning dominates plastic deformation.
- 5. The initial texture affects the deformation mechanism of specimens with different material orientations.

Acknowledgements

Ying Xiong gratefully acknowledges financial support provided by the Natural Science Foundation of China (Nos. 51775502, 51275472) and the Natural Science Foundation of Zhejiang Province (No. LY20E050024). Yanyao Jiang acknowledges the support from the National Science Foundation (CMMI-1762312).

References

- [1] Dudamell NV, Ulacia I, Gálvez F, Yi S, Bohlen J, Letzig D, Hurtado I, Pérez-Prado MT (2011) Twinning and grain subdivision during dynamic deformation of a Mg AZ31 sheet alloy at room temperature. Acta Mater 59:6949–6962
- [2] Wang BS, Xin RL, Huang GJ, Liu Q (2012) Effect of crystal orientation on the mechanical properties and strain hardening behavior of magnesium alloy AZ31 during uniaxial compression. Mater Sci Eng A 534:588–593
- [3] Jahedi M, McWilliams BA, Moy P, Knezevic M (2017) Deformation twinning in rolled WE43-T5 rare earth magnesium alloy: influence on strain hardening and texture evolution. Acta Mater 131:221–232



- [4] Knezevic M, Levinson A, Harris R, Mishra RK, Doherty RD, Kalidindi SR (2010) Deformation twinning in AZ31: influence on strain hardening and texture evolution. Acta Mater 58:6230–6242
- [5] Park SH, Hong SG, Lee CS (2013) In-plane anisotropic deformation behavior of rolled Mg-3Al-1Zn alloy by initial 10-12 twins. Mater Sci Eng A 570:149-163
- [6] Agnew SR, Tomé CN, Brown DW, Holden TM, Vogel SC (2003) Study of slip mechanisms in a magnesium alloy by neutron diffraction and modeling. Scripta Mater 48:1003–1008
- [7] Sarker D, Chen DL (2012) Detwinning and strain hardening of an extruded magnesium alloy during compression. Scripta Mater 67:165–168
- [8] He JJ, Liu TM, Zhang Y, Xu S, Lu LW, Tan J (2013) Deformation behaviour of hot extruded Mg alloy AZ31 during compressive deformation. Mater Sci Technol 29:177–183
- [9] Hong SG, Park SH, Lee CS (2010) Role of 10–12 twinning characteristics in the deformation behavior of a polycrystalline magnesium alloy. Acta Mater 58:5873–5885
- [10] Koike J, Ohyama R (2005) Geometrical criterion for the activation of prismatic slip in AZ61 Mg alloy sheets deformed at room temperature. Acta Mater 53:1963–1972
- [11] Song B, Xin RL, Chen G, Zhang XY, Liu Q (2012) Improving tensile and compressive properties of magnesium alloy plates by pre-cold rolling. Scripta Mater 66:1061–1064
- [12] Lou XY, Li M, Boger RK, Agnew SR, Wagoner RH (2007) Hardening evolution of AZ31B Mg sheet. Int J Plast 23:44–86
- [13] Xiong Y, Jiang Y (2016) Cyclic deformation and fatigue of rolled AZ80 magnesium alloy along different material orientations. Mater Sci Eng A 677:58–67
- [14] Gryguc A, Behravesh SB, Shaha SK, Jahed H, Wells M, Williams B, Su X (2018) Low-cycle fatigue characterization and texture induced ratcheting behaviour of forged AZ80 Mg alloys. Int J Fatigue 116:429–438
- [15] Yakubtsov IA, Diak BJ, Sager CA, Bhattacharya B, MacDonald WD, Niewczas M (2008) Effects of heat treatment on microstructure and tensile deformation of Mg AZ80 alloy at room temperature. Mater Sci Eng A 496:247–255
- [16] Al-Samman T, Gottstein G (2008) Room temperature formability of a magnesium AZ31 alloy: examining the role of texture on the deformation mechanisms. Mater Sci Eng A 488:406–414
- [17] Ando D, Koike J, Sutou Y (2010) Relationship between deformation twinning and surface step formation in AZ31 magnesium alloys. Acta Mater 58:4316–4324
- [18] Gryguc A, Jahed H, Williams B, McKinley J (2015) Mag-Forge—mechanical behaviour of forged AZ31B extruded

- magnesium in monotonic compression. Mater Sci Forum 828-829:291-297
- [19] Jiang J, Godfrey A, Liu W, Liu Q (2008) Microtexture evolution via deformation twinning and slip during compression of magnesium alloy AZ31. Mater Sci Eng A 483–484:576–579
- [20] Xiong Y, Yu Q, Jiang Y (2018) Deformation of extruded ZK60 magnesium alloy under uniaxial loading in different material orientations. Mater Sci Eng A 710:206–213
- [21] Gao P, Zhu SQ, An XH, Xu SQ, Ruan D, Chn C, Yan HG, Ringer SP, Liao XZ (2017) Effect of sample orientasion and initial microstructures on the dynamic recrystallization of a Magnesium alloy. Mater Sci Eng A 691:150–154
- [22] Chun YB, Davies CHJ (2011) Investigation of prism <a>slip in warm-rolled AZ31 alloy. Metall Mater Trans A 42:4113–4125
- [23] Xu DK, Liu L, Xu YB, Han EH (2008) The relationship between macro-fracture modes and roles of different deformation mechanisms for the as-extruded Mg–Zn–Zr alloy. Scripta Mater 58:1098–1101
- [24] Park SH, Hong SG, Lee JH, Lee CS (2012) Multiple twinning modes in rolled Mg-3Al-1Zn alloy and their selection mechanism. Mater Sci Eng A 532:401–406
- [25] Gryguc A, Shaha SK, Jahed H, Wells M, Williams B, Mckinley J (2016) Tensile and fatigue behavior of as-forged AZ31B extrusion. Frattura ed Integrità Strutturale 38:251–258
- [26] Gryguc A, Behravesh SB, Shaha SK, Jahed H, Wells M, Williams B, Su X (2019) Multiaxial cyclic behaviour of extruded and forged AZ80 Mg alloy. Int J Fatigue 127:324–337
- [27] Jiang L, Jonas JJ, Mishra RK, Luo AA, Sachdev AK, Godet S (2007) Twinning and texture development in two Magnesium alloys subjected to loading along three different strain paths. Acta Mater 55:3899–3910
- [28] Barnett MR, Keshavarz Z, Beer AG, Ma X (2008) Non-Schmid behavior during secondary twinning in a polycrystalline magnesium alloy. Acta Mater 56:5–15
- [29] Jiang L, Jonas JJ, Luo AA, Sachdev AK, Godet S (2006) Twinning-induced softening in polycrystalline AM30 magnesium alloy at moderate temperatures. Scripta Mater 54:771–775
- [30] Gryguc A, Behravesh SB, Shaha SK, Jahed H, Wells M, Williams B, Su X (2017) Monotonic and cyclic behaviour of cast and cast-forged AZ80 Mg. Int J Fatigue 104:136–149
- [31] Brown DW, Agnew SR, Bourke MAM, Holden TM, Vogel SC, Tomé CN (2005) Internal strain and texture evolution during deformation twinning in magnesium. Mater Sci Eng, A 399:1–12



- [32] Wu L, Agnew SR, Brown DW, Stoica GM, Clausen B, Jain A, Fielden DE, Liaw PK (2008) Internal stress relaxation and load redistribution during the twinning–detwinning–dominated cyclic deformation of a wrought magnesium alloy ZK60A. Acta Mater 56:3699–3707
- [33] Agnew SR, Brown DW, Tomé CN (2006) Validating a polycrystal model for the elastoplastic response of magnesium alloy AZ31 using in situ neutron diffraction. Acta Mater 54:4841–4852
- [34] Koike J (2005) Enhanced deformation mechanisms by anisotropic plasticity in polycrystalline Magnesium alloys at room temperature. Metall Mater Trans A 36:1689–1696
- [35] Ma Q, Kadiri HEl, Oppedal AL, Baird JC, Li B, Horstemeyer MF, Vogel SC (2012) Twins effects in a rod-textured AM30 magnesium alloy. Int J Plast 29:60–76
- [36] Jiang L, Jonas JJ, Luo AA, Sachdev AK, Godet S (2007) Influence of 10–12 extension twinning on the flow behavior

- of AZ31 Magnesium alloy. Mater Sci Eng A 445–446:302–309
- [37] Yi SB, Davies CHJ, Brokmeier HG, Bolmaro RE (2006) Deformation and texture evolution in AZ31 magnesium alloy during uniaxial loading. Acta Mater 54:549–562
- [38] Agnew SR, Duygulu Ö (2005) Plastic anisotropy and the role of non-basal slip in magnesium alloy AZ31B. Int J Plast 21:1161–1193
- [39] Wang L, Yang Y, Eisenlohr P, Bieler TR, Crimp MA, Mason DE (2009) Twin nucleation by slip transfer across grain boundaries in commercial purity titanium. Metall Mater Trans A 41:421–430

Publisher's Note Springer Nature remains neutral with regard to jurisdictional claims in published maps and institutional affiliations.

